Earth Systems, Resources, and Sustainability, 2026, 1(4), 364–380

Scilight Earth Systems, Resources, and Sustainability

Journal Homepage: https://www.sciltp.com/journals/esrs

Article

Porphyry Cu–Au and Cu–Mo Systems as Sources for Critical Metal Resources: A Review and Future Projection

Daniel Müller[1,*], David I. Groves[2,3], M. Santosh[2,4], Chengxue Yang[5] and Liang Zhang[2]

[1] Independent Researcher, Santiago 755000, Chile
[2] State Key Laboratory of Geological Processes and Mineral Resources, China University of Geosciences Beijing, Beijing 100083, China
[3] Centre for Exploration Targeting, University of Western Australia, Crawley, WA 6009, Australia
[4] Faculty of Science, Kochi University, Kochi 780-8520, Japan
[5] Institute of Earth Sciences and Resources, China University of Geosciences, Beijing 100083, China
[*] Correspondence: danielmuller33@yahoo.com

ABSTRACT

Porphyry systems are considered as low-grade, but high-tonnage, sources of scarce critical metals such as Cu and Mo, but they also host economic by-products of precious metals such as Au and Ag as well as rare trace critical metals such as Se, In, Te, and Re. The latter are of increasing importance as they represent essential components in the manufacture of green energy devices such as solar panels and modern high-tech gadgets. Until recently, the majority of critical trace metals remained in the metallurgical waste streams in most of the large porphyry mines, but several operators in Brazil, China and Japan have already begun to recover them from their mine tailings at an industrial scale. There are two sub-types of porphyry-type deposits: (1) porphyry Cu±Au, and (2) porphyry Mo±Re systems, the former associated with calc-alkaline or alkaline intrusions in continental- or island-arc settings, whereas the latter are normally hosted by more evolved high-K calc-alkaline intrusions derived in post-collisional arc settings. Both sub-types form large S and Fe, rather than Cu and Mo, anomalies in the Earth's upper crust and are defined by high total sulfide contents with pyrite representing the largest sulfide proportion when compared to the much less abundant directly economic chalcopyrite, bornite, and molybdenite phases. Importantly, pyrite hosts the majority of critical trace metals (Se, In, Te) in porphyry systems and therefore represents a vast untapped resource of these rare critical metals. Understanding the complex deportment of these rare critical elements can facilitate their extraction from pyrite concentrates in the metallurgical processing plants of current and future porphyry mining operations. This can boost their supply at a time when exploration discovery and mining of new porphyry systems have slowed due to a range of geological, governmental, environmental, and social issues and is unlikely to meet demand in the short term.

ARTICLE INFO

History:

Received 31 May 2026
Revised 10 July 2026
Accepted 27 July 2026
Published: 31 July 2026

Keywords:

porphyry Cu–Au–Mo mineral systems;
critical metals;
trace metal deportment;
mineral exploration

Citation:

Müller, D.; Groves, D.I.; Santosh, M.; et al. Porphyry Cu–Au and Cu–Mo Systems as Sources for Critical Metal Resources: A Review and Future Projection. *Earth Systems, Resources, and Sustainability* **2026**, *1*(4), 364–380. https://doi.org/10.53941/esrs.2026.100022

Research Highlights

- Porphyry systems represent a vast untapped resource of rare critical metals.
- They host essential components in the manufacture of green energy devices.
- Understanding complex deportment of rare critical elements is important to facilitate their extraction.

1. Introduction

The worldwide demand for critical metals is rising significantly mainly driven by population growth, new technological developments, and the proposed green energy transition [1–4]. Critical metallic mineral resources are defined by their natural scarcity, the potential disruption of their supply chains, and the ability to economically exploit them in an environmentally responsible manner [1]. As they are non-renewable resources in Nature, there are only two sources for the global supply of critical metals: (1) primary mining of mineral deposits, and (2) recycling of metals manufactured from those that were mined from mineral deposits.

At present, most critical metals cannot be recovered economically by recycling at industrial scale which leaves mineral exploration and mining as their main source, at least in the short term [3]. The manufacture of wind turbines, solar panels, and electric vehicles for the green energy transition requires increasingly large quantities of critical, including rare trace, metals [3, 5]. Rare critical trace metals such as Se, In, Te, and Re represent essential commodities in the electronics industry as well as for the manufacture of green energy devices. More specifically, Se is a key commodity for the production of Li–Se batteries, whereas Se, In, and Te are essential components in the manufacture of solar cells [6–9]. Rhenium is a critical trace element that is used in petroleum refining and electronics industries. It is also an important commodity for the manufacture of high-temperature resistant alloys [10].

However, these critical trace metals are very rare components of the Earth's crust and generally do not form economically mineable deposits on their own. Instead, they only occur as rare by-products of large base-metal deposits such as porphyry-, SEDEX- and MVT-type mineral systems [11]. Importantly, global geopolitical tensions as well as the critical metals natural scarcity, heterogeneous geographical distribution, and a variety of social issues pose significant challenges for the future maintenance of stable industrial supply chains.

Hence, it is of increasing importance to better understand the geochemical trace element composition, deportment of these trace elements, and economic potential of these critical metal systems to enable the efficient metallurgical extraction of trace critical metals in the future.

Porphyry systems are large-tonnage, but low- to medium-grade, deposits that have significant economic importance, having supplied not only approximately three-quarters of global Cu, half of Mo, and one-fifth of Au, but also substantial quantities of other critical metal by-products such as Ag, Sn and W over the past century [12–15]. Due to their high pyrite contents, porphyry systems are often regarded as giant S and Fe, rather than Cu and Mo, anomalies in the Earth's upper crust [16–18].

Two sub-types of porphyry systems may be distinguished: (1) porphyry Cu±Au [19]; and (2) porphyry Mo deposits [20]. The former is commonly hosted by oxidized intrusions with intermediate compositions, while the latter are associated with highly evolved and commonly high-K intrusions [13, 19, 20].

Large porphyry Cu and Mo systems may contain millions of tons of Cu and/or Mo in small rock volumes on the order of a cubic kilometre, enriched in concentration by two to three orders of magnitude compared to their average wall rocks [21]. However, porphyry Cu–Au and Mo systems also host rare critical trace metals such as Se, In, Cd, Te and Re that are in high demand for the green energy transition as well as for the manufacture of modern high-tech gadgets [22–29]. Significant concentrations of critical trace metals such as Se, In, Te and Re may remain in the waste streams of large porphyry mines, and, until recently, have often not been recovered alongside the primary metals [28, 30]. However, due to the increasing demand for these critical trace metals, several operators in Brazil, China and Japan have begun to recover critical metals from metallurgical waste and mine tailings using advanced hydrometallurgical techniques [31–34].

This study reviews the important role of porphyry systems as a global source for critical metals such as Cu, Mo, Pd, Ag, Sn, W, and Au [13, 14] as well as rare trace metals such as Se, In, Te, and Re [22–29, 35, 36].

2. Porphyry Cu±Au Systems

Porphyry-related mineral systems are documented worldwide at subduction-related convergent margin settings that include volcanic and island arcs (Figure 1: [37–39]), particularly where there is an extended and/or complex subduction history [13, 21, 40, 41]. Porphyry Cu±Au and associated high-sulfidation epithermal precious-metal

and skarn deposits are the most prominent mineral systems formed during the evolution of convergent margins [42]. Individual clusters of porphyry Cu±Au systems are normally sited along extensive curvilinear segments of volcanic arcs such as the Andes (Figure 2: [14, 43]) at spacings of about 10s to 100s of km [44], especially where they are intersected by deep-seated lineaments [41, 45, 46] such as in the giant Chuquicamata-Radomiro Tomic-El Abra [47, 48] and Escondida porphyry clusters in northern Chile [49, 50].

Other significant porphyry Cu–Au districts are documented in island arc-settings such as the southwest Pacific (Figure 1) that comprises over 160 early- to middle-Miocene and Pliocene-Pleistocene Au-rich porphyry systems [39]. Importantly, the majority of Au-rich porphyry systems such as Grasberg, Indonesia [51], Northparkes and Cadia, both New South Wales, Australia [52], Oyu Tolgoi, Mongolia [53], and Pebble, Alaska [54] are recorded from island arc or post-collisional arc-settings. Other porphyry Cu±Au systems related to continent-continent collision are documented in the post-collisional Tethyan belt (Figure 3) ranging from Iran to Tibet [55–57]. Although porphyry Cu–Au deposits are significant global sources of copper and gold, they also contain minor metallic elements as trace by-products as discussed further below.

Porphyry Au±Cu systems are normally hosted by high-K calc-alkaline to alkaline (e.g., shoshonitic) intrusions [52, 58, 59]. They typically occur in zones of complex subduction geometry due to multiple events involving polarity reversals, arc-arc and island arc-continent collisions, rifting, and transcurrent faulting [39, 52]. As in the Andes, porphyry Cu–Au clusters such as Oyu Tolgoi, Mongolia, are related to bends and tears in down-going subduction slabs, especially near high-angle arc-transverse faults intersecting the arcs [41, 45, 53, 60]. Porphyry systems in island arc-settings are commonly hosted by less evolved and distinctly potassic, or even alkaline, monzodioritic or monzonitic intrusions [52, 58, 59].

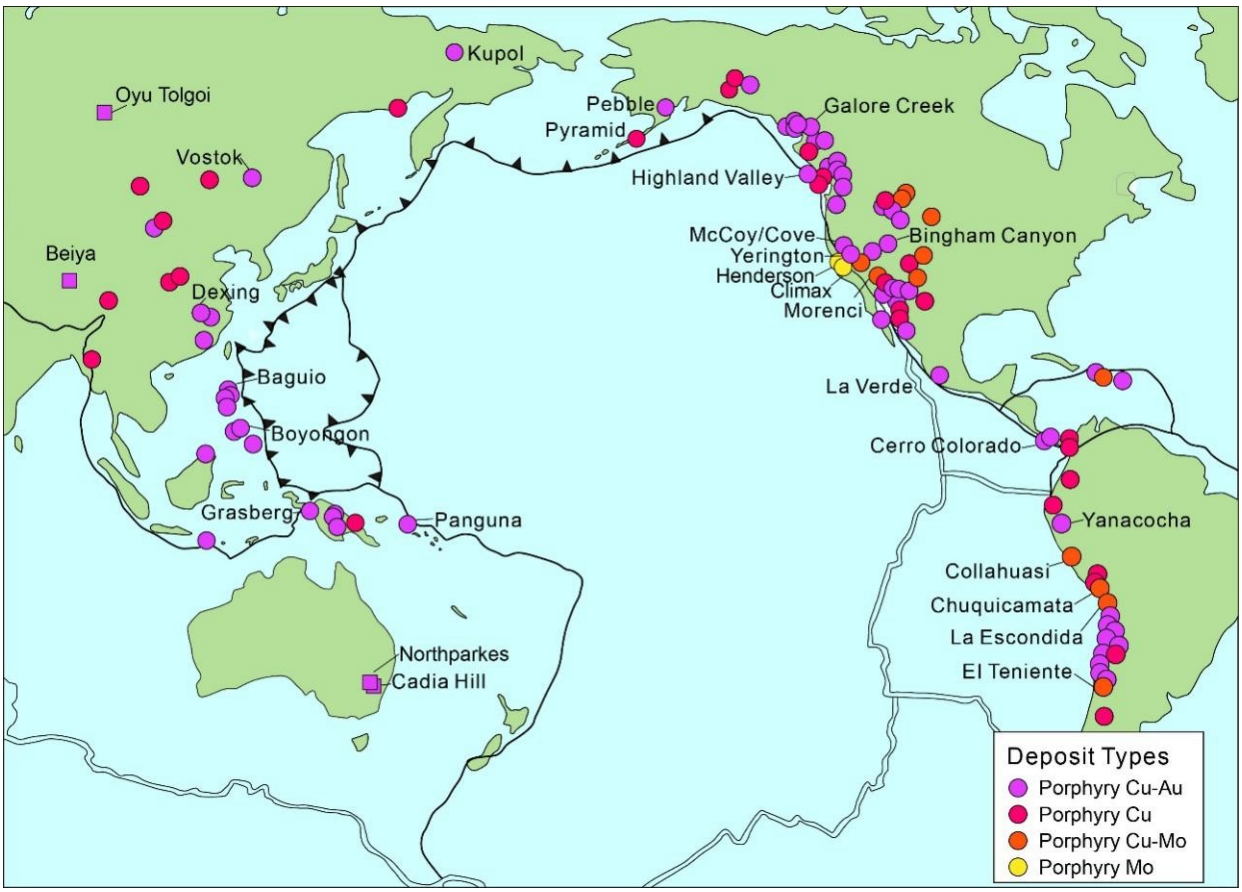

Figure 1. Distribution of porphyry systems in volcanic and island arcs across the Pacific Ocean: adapted from [37, 38] with data from the SW Pacific derived from [39]. Square symbols are important deposits not related to tectonics directly related to Pacific and Paleo-Pacific Ocean Plates.

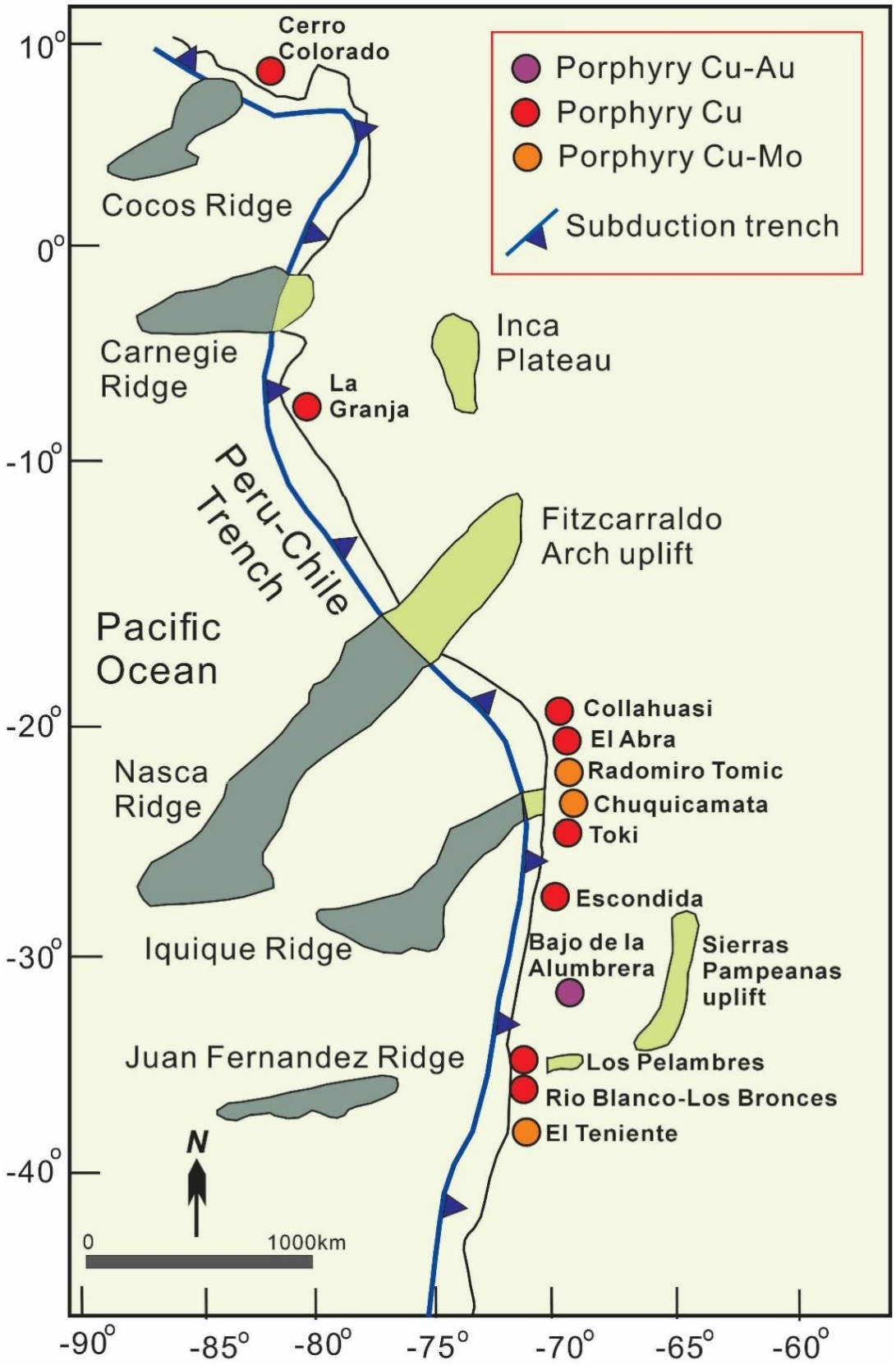

Figure 2. Distribution of porphyry systems across the South American Andes. Porphyry Cu–Au deposits are shown in purple, porphyry Cu deposits in red, and porphyry Cu–Mo deposits in orange. Adapted from [37, 43] with original data largely from [14, 46].

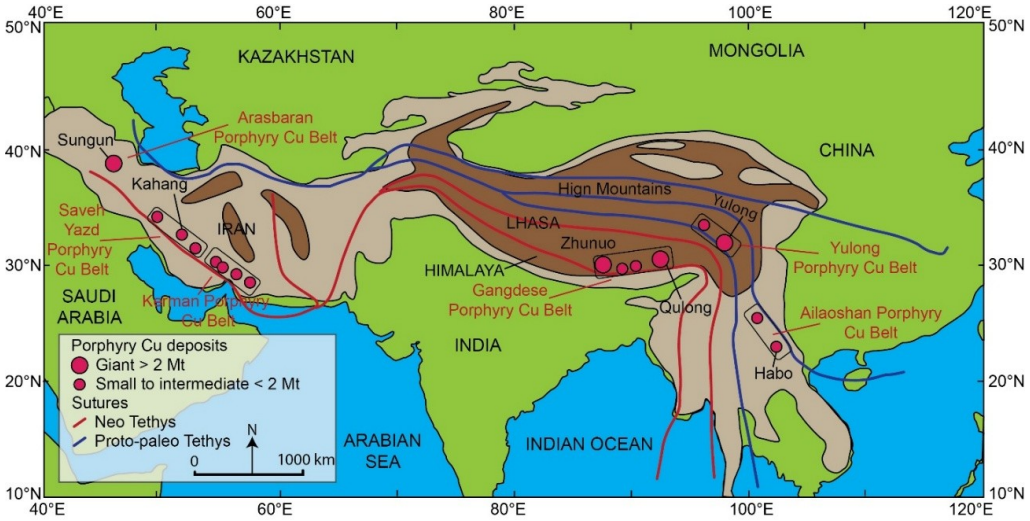

Figure 3. Schematic map of the eastern Tethyan domain, showing Tethyan sutures and post-collisional porphyry Cu±Au or Mo belts with the largest giant deposit (>2 Mt Cu) named. Simplified from [61] who provide sources for their figure. Dark brown = highest mountain belts that include the Himalaya. Pale brown = mountain belts; Green = lowlands and high plains.

3. Porphyry Mo Systems

Continental collision and/or post-collisional settings often generate large to giant, but low-Re, porphyry Mo systems, such as in the Altaid/Transbaikal-Mongolian collage and the North China Craton [62]. Figure 3 represents a schematic map of the eastern Tethyan domain with the main Tethyan sutures and post-collisional porphyry Cu±Au or Mo belts with the largest giant deposit (>2 Mt Cu within each belt) named [61]. They commonly contain distinct unidirectional solidification (UST) textures [63] and are related to magmas derived from partial melting of old continental crust. By contrast, intracontinental or back-arc rifts, which are associated with extensional regimes, may produce high-F and high-grade Mo deposits, for example, Climax and Henderson in Colorado, USA (Figure 1), considered as type examples of porphyry Mo systems [64].

China also hosts porphyry Mo deposits that are external to the North China Craton in the eastern Qinling porphyry Mo cluster and in the Xing'an range [63, 65, 66]. The mineralization consists of molybdenite that occurs disseminated or within quartz stockwork veins and related hydrothermal breccias [67] hosted by strongly evolved, F-rich, high-K calc-alkaline intrusions [62, 66, 68, 69]. Their parental granodiorite or monzogranite stocks are locally accompanied by contemporaneous mafic, and commonly high-K, trachybasaltic to trachyandesitic dikes [20]. Parental intrusions typically measure several hundred meters in diameter and have cylindrical sub-vertical shapes. Their root zones typically extend into deep underlying, parental batholiths [20]. Many porphyry Mo deposits are spatially associated with related skarn systems [66, 69, 70].

4. Genesis of Porphyry Systems

Porphyry Cu systems can be hosted by calc-alkaline [19] or high-K calc-alkaline to alkaline intrusions [59]. The empirically more common calc-alkaline porphyry systems have no specific igneous rock association, with fertile intrusions ranging from diorites to granodiorites [19]. By contrast, Au-rich porphyry Cu systems are normally hosted by high-K or alkaline intrusions that can range in composition from monzodiorites through monzonites to quartz-monzonites [58, 59]. Porphyry Mo systems are normally hosted by strongly fractionated high-K calc-alkaline intrusions that can range from granodiorites to monzogranites.

In both sub-types, porphyry-style mineralization and its parental intrusions form by low-degree partial melting of metasomatized, LILE-, volatile-, and H_2O-enriched, mantle lithosphere in arc settings [71–74]. The higher gold contents of high-K or shoshonitic porphyry systems [58, 59] as well as zircon mineral compositions from fertile porphyry systems support this model [75]. Adiabatic decompression melting of these enriched mantle lithosphere domains (Figure 4; [76, 77]) can produce ascending basic H_2O-rich magmas with high oxidation states [15, 20, 78]. These ascending melts can subsequently form magma chambers in the shallow crust where ongoing crystal fractionation and the continued replenishment by additional injections of more basic mantle melt leads to the release of evolved magmatic pulses from the top part of the chamber [79, 80]. Pulses of fertile magma released from the top of this fractionating magma chamber are capable of forming economic porphyry systems at shallow depths of 3–5 km beneath the paleo-surface [21, 81]. The porphyry-type mineralization forms in response to focused expulsion of metal-bearing, saline fluids from the cooling magma chamber [82]. A restricted zone of ore-mineral precipitation within a more extensive plume of fluid up-flow is thought to be the key to economic metal accumulation [21, 82]. The ore bodies typically have bell-like or cylindrical shapes (Figure 5), centered on stocks or plugs of porphyritic intrusions emplaced above cupolas in the roof of magma chambers [82]. This commonly results in a cluster of porphyry intrusions,

including both mineralizing and barren porphyry stocks, that cut their underlying host batholith, and are emplaced into the overlying volcano-sedimentary units [21]. The top of the ore shell is commonly abrupt and coincides with the top of a dense vein network, indicating that fluid pressures were sufficient to induce hydraulic fracturing [82].

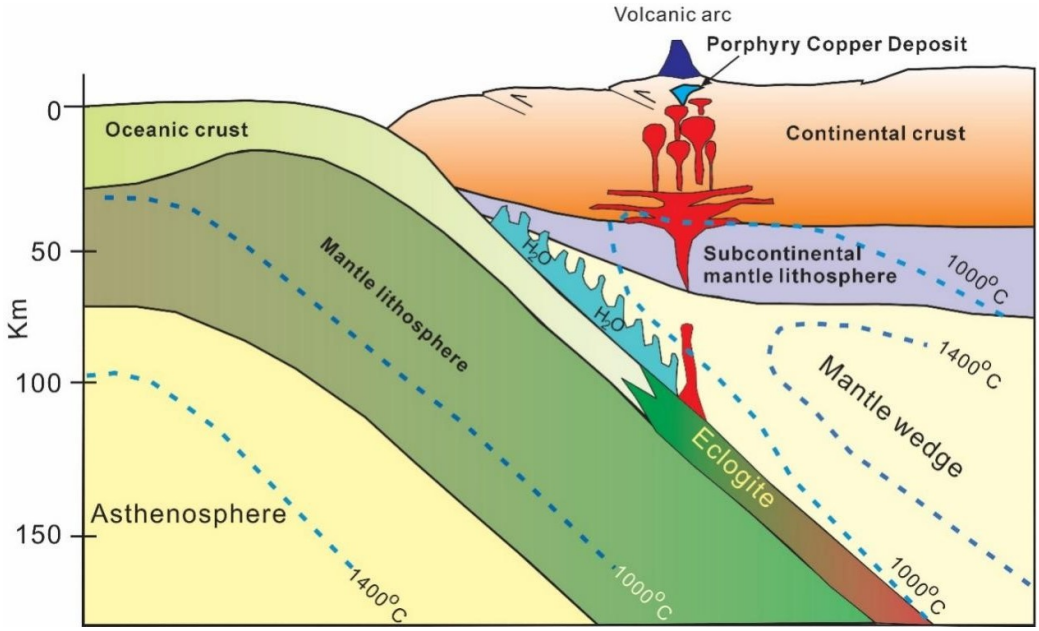

Figure 4. Geological sketch model of a subduction zone (mature continental arc) illustrating the genesis of porphyry systems (PCDs). Dehydration of the subducted oceanic slab is shown in light blue and zones of partial melting and the emplacement of intrusions in the crust are shown in red. Note that porphyry systems occur in clusters above fractionating magma chambers in the upper crust, but the majority of them are uneconomic or barren. After [76, 77].

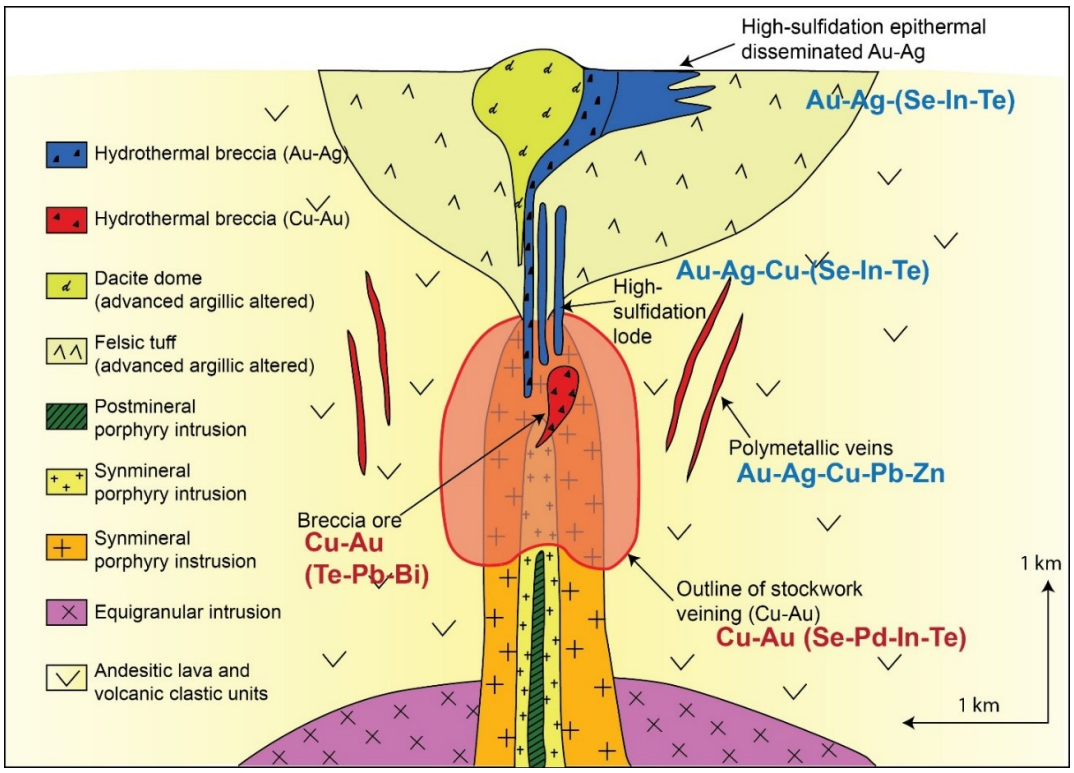

Figure 5. Geological sketch model of a porphyry Cu–Au system highlighting the occurrence of critical metals. Porphyry-style mineralization is shown in red and related high-sulfidation style mineralization is shown in blue. Note that most porphyry systems are formed from numerous syn-mineral intrusive phases as indicated in the Figure. Multiple syn-mineral intrusions can add to the vein densities and thus improve the grades. After [13].

Importantly, the intrusive stocks or cupolas associated with porphyry Cu–Au systems are generally oxidised [77, 83, 84]. Porphyry Cu–Au deposits have systematically higher oxygen fugacities and FeO contents compared to porphyry Mo deposits [14]. At constant temperatures, as the oxidation state increases, the concentration of dissolved sulfide (S^{2-}) in the melt decreases, whereas the dissolved sulfate (SO_4^{2-}) increases as sulfur is oxidized [85, 86]. Thus, the potential for early precious metal segregation into magmatic sulfide phases is reduced [85]. If the sulfide concentration in the melt is reduced, Au and Cu can be concentrated in the volatile-enriched top part of the magma chamber [85]. Once volatile saturation occurs during secondary boiling, the magma chamber releases pulses of metal- and volatile-enriched melts that can form porphyry Cu–Au mineralization in the upper crust [87]. High oxidation states of a melt are generally correlated with high magmatic H_2O contents [88]. In arc systems, mantle oxidation by subducted H_2O and Fe^{3+} can lead to complete consumption of sulfide, so that partial melting may take up all available Cu and Au [21].

Geochemically, porphyry systems represent natural vertical pumps of hot hydrothermal fluids within the upper crust [21] that are defined by both lateral and vertical alteration mineral and geochemical zonation [89] ranging from central Cu–Au cores toward peripheral Ag–Zn–Pb assemblages, as well documented from porphyry Cu–Au systems (Figure 5). As illustrated in Figures 5 and 6 [90], all porphyry systems are spatially associated with zoned hydrothermal alteration assemblages including sodic-calcic alteration of their root zones grading into central potassic alteration zones that are surrounded by peripheral propylitic alteration assemblages [21]. Sericitic and argillic alteration zones commonly lie above the potassic alteration core, with all overlain by a lithocap comprising an advanced argillic altered andesitic or dacitic carapace [91]. In places, structurally controlled sericite alteration can overprint the earlier potassic alteration assemblage.

This hydrothermal alteration zonation reflects the cooling of magmatic-hydrothermal fluids from $<$700 °C to $<$250 °C [92] with the evolution of high-temperature two-phase and highly saline fluids [21]. The complex formational and emplacement history of porphyry systems means that both mantle and crustal elements can be enriched in the hydrothermal metal-bearing fluids. Critical metals are precipitated as sulfide phases such as minor bornite and chalcopyrite, and abundant pyrite occurring both as disseminations within the parental intrusion and their wall rocks and/or in cross-cutting stockwork-type quartz vein networks [21, 92, 93].

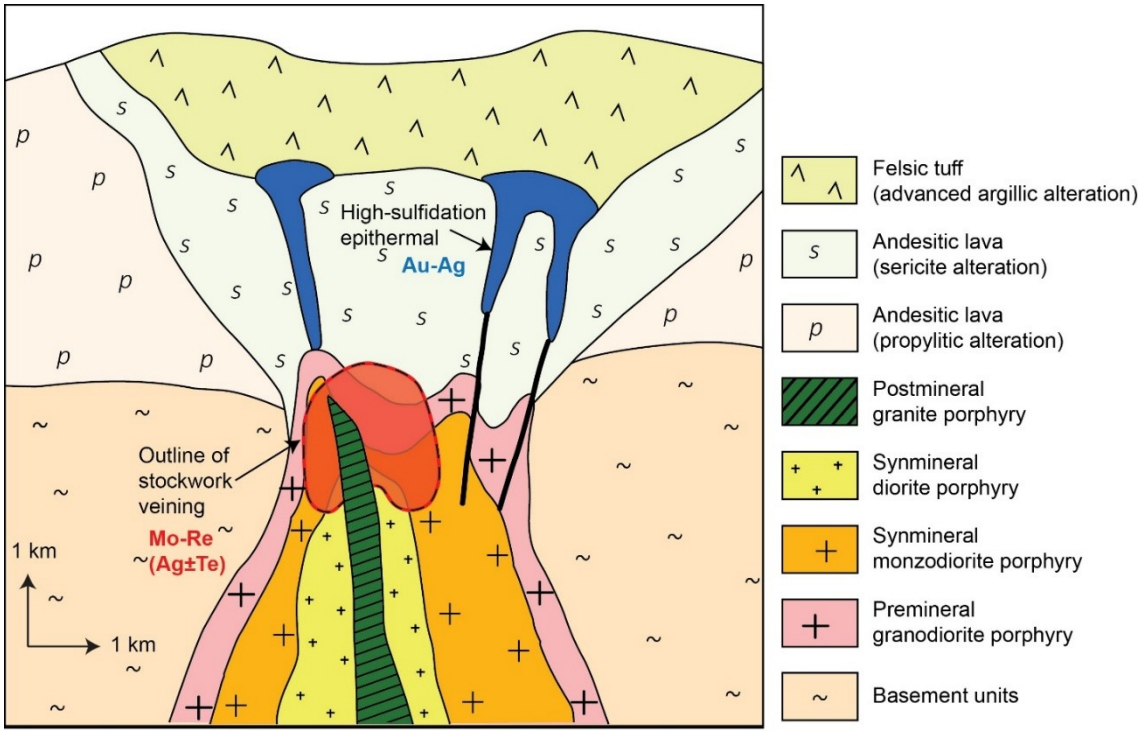

Figure 6. Geological sketch model of a porphyry Mo±Re system highlighting the occurrence of critical metals. Porphyry-style mineralization is shown in red and related high-sulfidation style mineralization is shown in blue. Note that most porphyry systems are formed from numerous syn-mineral intrusive phases as indicated in the Figure. Multiple syn-mineral intrusions can add to the vein densities and thus improve the grades. In some porphyry systems, the underlying magma chamber keeps fractionating after the release of the syn-mineral intrusions as documented by the emplacement of evolved and barren post-mineral intrusions which can stope out the porphyry mineralization (shown in green). After [90].

Porphyry systems form at shallow depths in the upper crust during compressive stress regimes [21, 94]. Exhumation and secondary oxidation and enrichment by circulating groundwaters finally determine the economics of a deposit, hence both representing critical factors in the formation of economic porphyry systems [21]. More specifically, calculations for different major porphyry Cu–Au systems using thermochronology by McInnes et al reveal uplift rates of about 0.26 to 0.72 km per million years [95]. This might explain why preserved porphyry systems only rarely extend back beyond the Miocene with most of the older, Mesozoic, examples recorded from post-collisional arcs such as Pebble, Alaska [54]. However, more rarely, there are also sub-economic examples recorded from Archean greenstones belts in the Pilbara [96] and Yilgarn Cratons in Western Australia [97].

5. Critical Metal Contents of Porphyry Systems

The proclaimed green energy transition has also led to a rapidly increasing demand for scarce critical metals such as Cu and Mo, the major economic critical metals in porphyry systems, which are essential commodities in the electronic, steel, and construction industries [98, 99]. Rare trace critical metals such as Se, Cd and Te are essential commodities for the manufacture of green energy devices such as solar panels and Li–Se batteries [100–102] as well as for the production of semiconductors [103]. However, the low average crustal abundance of Se, Cd, Te and Re of $<$0.05 ppm [104, 105] and the fact that those trace critical metals do not form their own minerals, but are only present in trace amounts in sulfide minerals such as pyrite and chalcopyrite that are exploited in major base-metal deposits such as porphyry systems, poses a dilemma for global supply chains [11].

Importantly, the rapidly increasing industrial demand for trace critical metals that had traditionally been lost in the metallurgical tailings of large base-metal mining operations [30, 36] has put them into the focus of attention. Hence, several operators in Brazil, China and Japan have begun to recover trace metals such as REEs, Ga and Ge from metallurgical waste and mine tailings [31–34].

Importantly, recent studies reveal that porphyry systems are important sources of trace critical metals such as Se, Te and Re (Figures 5 and 6), even though the factors controlling their enrichment still remain poorly understood [22, 23, 29, 102, 106, 107]. However, Jin et al document that the elevated oxidation states and high H_2O contents of arc magmas may lead to a higher Se and Te fertility [29].

5.1. Critical Metal Content of Porphyry Cu–Au Systems

Porphyry Cu±Au systems are the global main sources of Cu and also produce over 20 vol% of Au [13]. In porphyry systems, Cu and Au are hosted by sulfide phases such as bornite and chalcopyrite. More rarely, Au can also be sited in pyrite or secondary magnetite phases.

However, porphyry Cu–Au systems may also contain significant by-products of precious metals such as Ag, Pd, and Pt [14, 15, 108], especially in alkaline systems, as well as trace critical metals such as Se, In, Te, and Bi (Figure 5) that are mostly lattice-bound or more rarely hosted as micro-inclusions within sulfide phases such as pyrite, chalcopyrite, bornite and galena within several different parts of the zoned porphyry system [22, 24, 28, 29, 107].

The metallurgical processing of copper ore can produce significant by-products of Te [26]. Bornite, one of the most important Cu-bearing phases in porphyry systems, represents a major host for Se, Ag, Te, and Bi, whereas chalcopyrite can locally host significant Se contents of up to 310 ppm [109, 110]. However, until recently, copper concentrates commonly incurred monetary penalties from the smelter if they contained in excess of 500 ppm Se [110]. Chalcopyrite phases from the giant Chuquicamata porphyry Cu–Mo deposit, Chile, host high concentrations of trace metals of up to 22,000 ppm Se, 68 ppm Sn, 45 ppm Ag, and 22.8 ppm In [24]. Importantly, the highest concentrations are recorded from chalcopyrite phases collected within the potassic altered core of the porphyry system [24]. More specifically, high concentrations of Se and In within chalcopyrite phases are related to the high temperature background potassic alteration, with lower concentrations of these two elements associated with the lower temperature quartz-sericite and chlorite alteration zones [24]. Recent mineralogical studies at the Rio Blanco porphyry Cu–Au deposit in northern Chile reveal Te enrichments of the Cu ore to levels of up to 300 times average crustal abundance [28].

Highly evolved and granite-hosted porphyry Cu systems may also contain significant by-products of rare critical metals such as Sn and W [12, 111], that are also known as trans-porphyry type deposits documented within continental plates and resulting from large-scale shearing between cratons [112]. In those deposits, Sn occurs in cassiterite and W in wolframite phases.

In porphyry Cu–Au systems of the Metaliferi Mountains, Romania, galena forms micro-inclusions within pyrite, chalcopyrite and bornite phases locally containing significant trace element concentrations of up to 17,380 ppm Se, 3750 ppm Ag, 1570 ppm Ge and 780 ppm Te [22], although concentrations will be orders of magnitude lower in the copper ores.

5.2. Critical Metal Contents of Porphyry Mo Systems

Although Mo is also derived as a by-product from large porphyry Cu±Mo deposits such as Bingham, USA [113], or Chuquicamata, Chile [47], the most significant resources are hosted by porphyry Mo systems (Figure 6) that also represent the world's largest source of Re [24, 35, 62, 114]. Major trace metals and elements associated with porphyry Mo deposits include Ag, Sn, W, Re, Au, and Bi, commonly appearing in trace quantities within

molybdenite or as discrete associated minerals [65]. Gold and Ag may also be concentrated in high sulfidation epithermal vein systems above the Mo ore bodies (Figure 6). These deposits, which account for over 95% of the global molybdenum supply, are commonly hosted in felsic, highly evolved, fluorine-rich granites (e.g., Climax-type) granites [20, 62].

The Re contents in molybdenites from porphyry Mo deposits in the North China Craton are mostly higher than 100 ppm [62] thus indicating a crust-dominant source [115]. The Re contents in molybdenites from porphyry Mo systems in NE China are highest in the older systems with molybdenites from the Early Paleozoic Duobaoshan-Tongshan district containing maximum Re contents of up to 1000 ppm [62]. Berzina et al also document significant Re concentrations in molybdenite concentrates from the Aksug (460 ppm) and Erdenetuin-Obo (199 ppm) porphyry Mo–Cu deposits in Siberia [35]. Molybdenites from some Greek porphyry Mo–Cu deposits have exceptionally high Re contents ranging from 7260 to 42,100 ppm [114, 116]. Due to the large size of porphyry-type deposits, their total Re contents can be economically significant and the giant Pebble deposit, Alaska, contains as much as 4000 t Re [114]. Molybdenite commonly hosts trace elements including Re, Cu, Se, Te, W, Pb, and Bi, in addition to Re, in its lattice or as nano-inclusions. The strong geochemical correlation between Mo and Re in deep drill core samples suggests the substitution of Mo by Re within molybdenite [102] predominantly through lattice substitution [117]. Recent studies on the Jinduicheng porphyry Mo deposit in the Dabie Mo belt, Qinling Province, China, suggest that Re preferentially partitions relative to Mo into the vapor phase and precipitates later during cooling, resulting in late-stage, Re-rich molybdenite [117].

Tungsten and Bi are commonly present, particularly in W-Mo porphyry and related skarn systems, where they may be recovered as a by-product [65, 70, 118]. Elevated concentrations of Nb, Ta, and REE are documented from alkali-feldspar monzogranite-hosted porphyry Mo deposits [119, 120].

Although Se has been mainly documented from chalcopyrite phases in porphyry Cu–Au systems [110], it is also reported from chalcopyrite-free porphyry Mo deposits where it is hosted by pyrite [121]. Mineralogical studies on pyrites from the Lakang'e porphyry Mo deposit in Tibet document up to 147 ppm Se in pyrite [121].

6. Deportment of Critical Trace Elements in Sulfide Components of Porphyry Systems

Porphyry systems are widely regarded as giant S and Fe, rather than Cu and Mo, anomalies in the Earth's upper crust due to their high pyrite contents [16–18]. The pyrite contents of porphyry systems normally increase from a pyrite-poor, but chalcopyrite- and/or molybdenite-rich potassic core (Py:Cpy $<$ 1) through a phyllic zone (Py:Cpy ratios $\sim$1) into the surrounding 'pyrite shell' where the pyrite contents can be locally up to 5 vol%, the latter representing important IP anomalies for exploration [122]. More specifically, the pyrite content at the Santa Rita porphyry Cu deposit, New Mexico, increases from $<$1 wt% pyrite in the central part of the ore body, through a surrounding zone with 1–4 wt% pyrite to an outer zone with $>$4 wt% [122, 123]. By contrast, the greatest chalcopyrite content, $>$0.4 wt% chalcopyrite, is recorded in the zone with intermediate amounts of pyrite. Inward from this higher chalcopyrite zone, the chalcopyrite decreases to about $<$0.1 wt%, whereas outward from the higher-grade zone it ranges between 0.1 and 0.4 wt% [122, 123]. Similar observations on the relative proportions of sulfide phases are recorded from the El Salvador porphyry Cu deposit, Chile [124]. At the Bingham porphyry Cu–Au deposit, Utah, there are five overlapping, but concentric, zones from the center outward: (1) a low-grade sulfide core with $<$0.5 wt% of pyrite, chalcopyrite, bornite, and molybdenite, (2) a molybdenite, bornite + chalcopyrite zone, (3) a chalcopyrite + pyrite zone, (4) a pyrite-dominated zone, and (5) a galena + sphalerite zone [122, 125]. As at Santa Rita, at Bingham the inner zone contains rare pyrite, the Cu ore body contains 1–2 wt% pyrite, and the surrounding pyrite shell can exceed 4 wt% [122, 125]. In summary, the pyrite/chalcopyrite ratio is lowest in the potassic alteration zone and highest in the phyllic alteration assemblage of porphyry systems. Hence, understanding the sulfide mineralogy is vital in the efficient metallurgical treatment of the ore.

The main economic metals Cu, Au, and Mo are almost exclusively present as discrete grains or grain intergrowths of Cu sulfides, native Au/electrum, Au–Ag tellurides, and molybdenite, respectively [25, 26, 122]. Precious metals such as Au and Ag may also be concentrated as inclusions or along fracture surfaces in pyrite from porphyry Cu–Au systems [25]. In porphyry Cu–Au systems, the deportment of trace critical metals such as Se and Te is preferentially within the crystal lattice of bornite, chalcopyrite or zoned pyrite phases as recently documented [25, 26, 126, 127]. Their complex deportment within individual pyrite grains can take various geometric forms as demonstrated in Figures 7–9. However, in places, Te may also occur in rare telluride phases that can form micro-inclusions within sulfide phases or more rarely discrete telluride minerals intergrown with them (Figure 10: [27]).

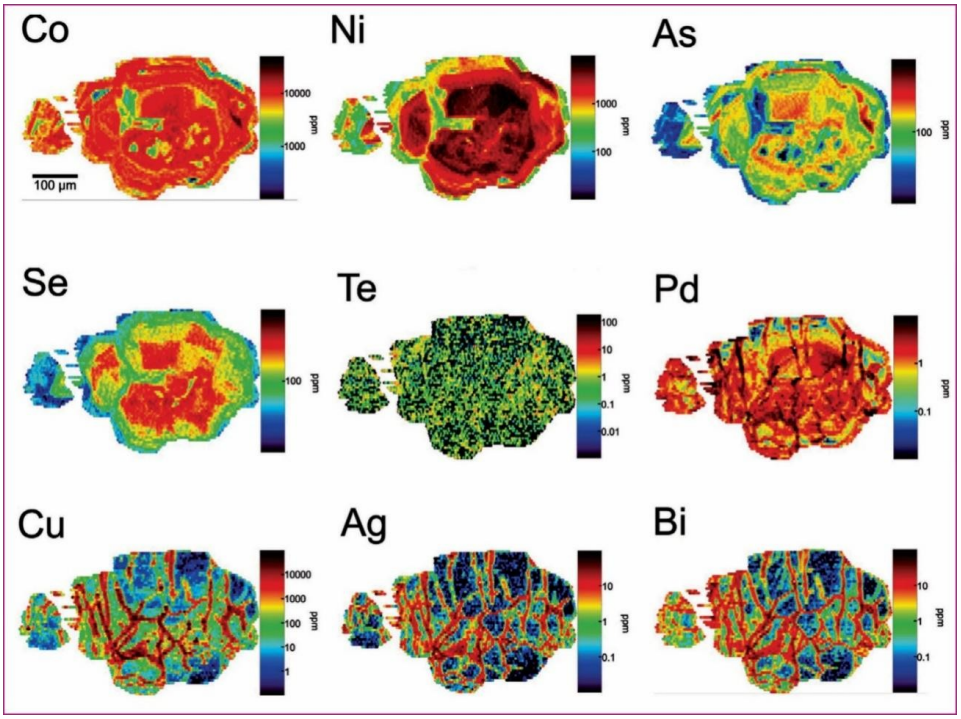

Figure 7. LA-ICP-MS scans of trace element concentrations in late-stage pyrite phases from the Afton porphyry Cu–Au deposit, British Columbia, Canada. Selenium and Pd are concentrated in primary growth zones in the pyrite. Abundant fractures are infilled by chalcopyrite and coincide with enrichments in Cu, Bi, and Ag. However, Cu is mainly hosted by bornite and chalcopyrite phases. From [127].

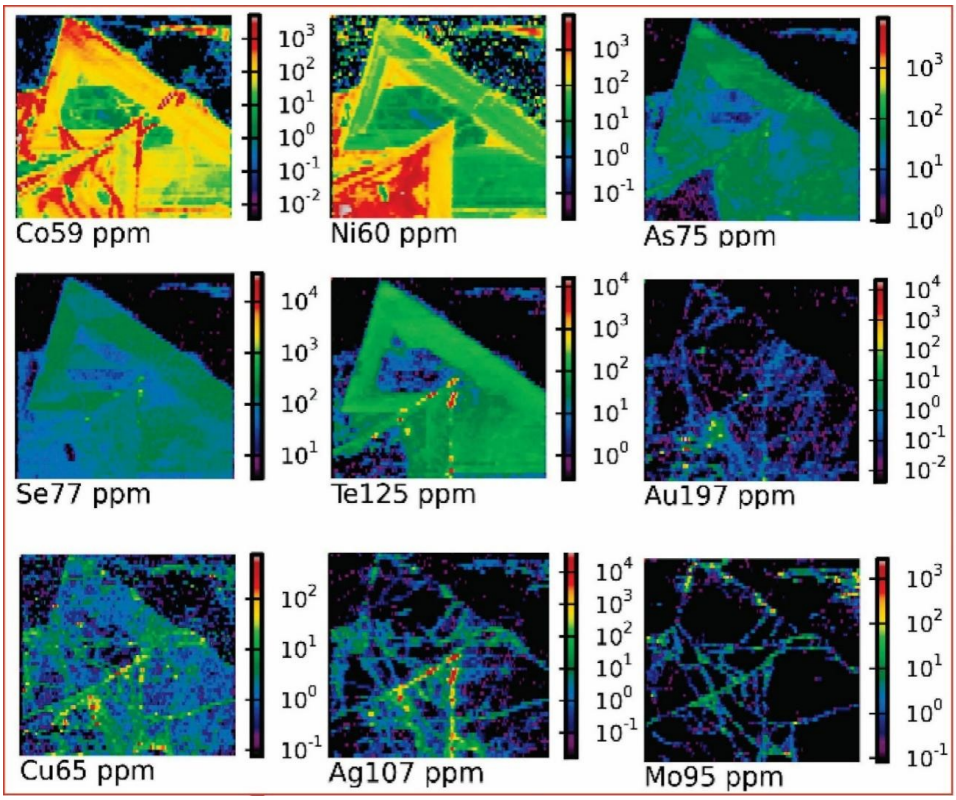

Figure 8. LA-ICPMS trace element scans of pyrite from the Kasier-Boda porphyry Cu–Au deposit, New South Wales, Australia. The pyrite grain has been fractured, and these fractures contain chalcopyrite and Au–Ag tellurides. After [25] with Copyright from Elsevier.

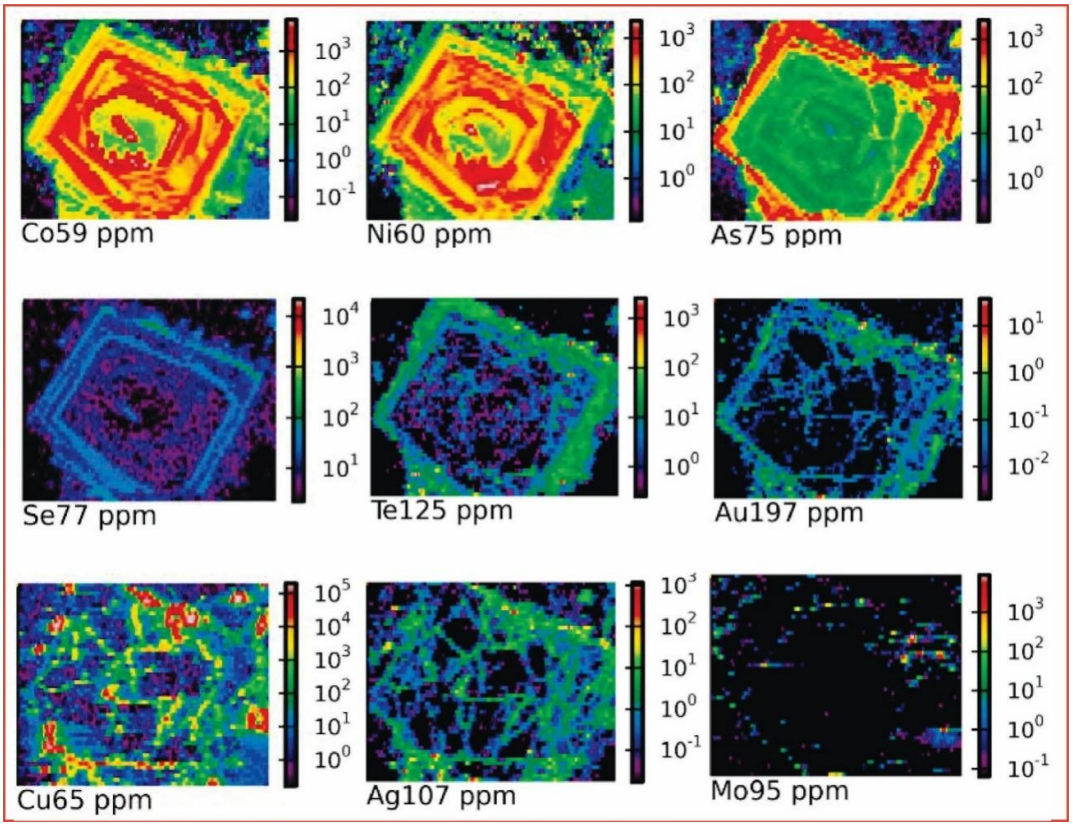

Figure 9. LA-ICPMS trace element image of pyrite from the Theia porphyry Cu–Au–Mo prospect, New South Wales, Australia. Pyrite in this sample contains abundant inclusions of both sulfide and non-sulfide minerals such as silicates and carbonates. Fractures overprint the grain. After [25] with Copyright from Elsevier.

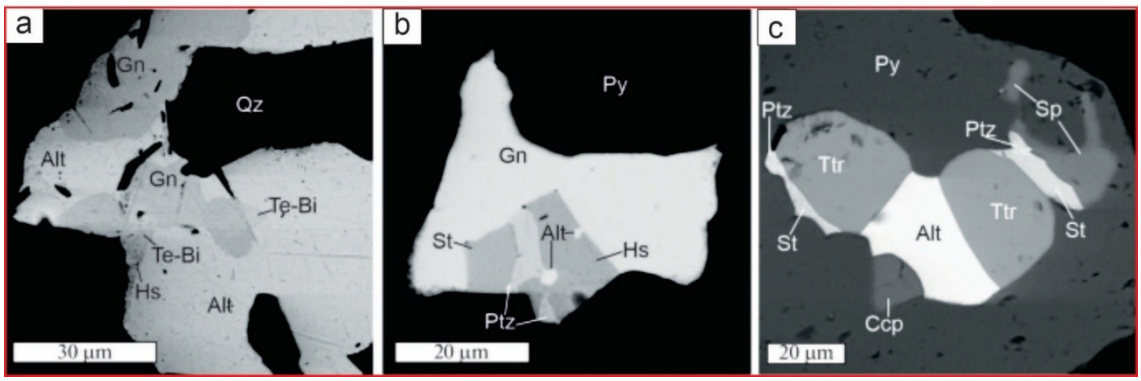

Figure 10. (A) intergrowths of hessite, telluro-bismuthite Bi_2Te_3 (Te–Bi), and galena in altaite within quartz; **(B)** intergrowths of galena, stuttzite, hessite, petzite, and altaite in pyrite phases; **(C)** intergrowths of altaite, tetrahedrite, sphalerite, petzite, and stützite in pyrite phases from the Birgilda porphyry Cu deposit in southern Urals, Russia. From [27] with Copyright from Pleiades Publishing Ltd.

Importantly, pyrite represents the largest percentage (40–80 vol%) of the sulfide phases in porphyry Cu–Au deposits, whereas chalcopyrite only represents 0.4–3.0 vol% [122, 123, 125], with bornite normally not exceeding 2.0 vol% even in alkaline porphyry Au systems [58], which means that the majority of critical trace metals for solar panels, wind turbines and electric vehicles such as Se, In, and Te can be dominantly hosted in pyrite, at least in porphyry systems.

Mineralogical studies on pyrite from the Elatsite porphyry Cu–Au deposit, Bulgaria, reveal high, but variable Se contents ranging from 34.4 to 393.3 ppm, while Te ranges from 1.1 to 16.8 ppm [126]. Mineralogical studies on the trace metal content of sulfide phases from the giant Bingham porphyry Cu–Au deposit, Utah, USA [26] reveal that Se and In may be hosted along structural cracks in chalcopyrite, whereas bornite and digenite host Se, In, and Te in their lattice structure. At Bingham,

pyrite contains the highest Se concentrations (>700 ppm) of the sulfide phases [26]. Even more recent studies on pyrite phases from the New Afton porphyry Cu–Au deposit in British Columbia, Canada [127] reveal significant Pt contents of up to 24 ppm in pyrite crystal cores (Figure 7) that are Co-rich (>1.0 wt%), but Se-poor. The incorporation of Se into pyrite is documented to be strongly temperature dependent [127, 128]. Selenium also shows the largest oscillations in concentration (up to 5 orders of magnitude) in pyrite phases (Figures 8 and 9) due to a wide variety of thermochemical parameters [25], particularly in high-temperature magmatic-hydrothermal mineralization types such as porphyry Cu–Au systems [127, 129]. In Cu-dominated hydrothermal mineral systems, Se is preferentially hosted in bornite and chalcopyrite phases as recorded from porphyry Cu–Au as well as VMS-type polymetallic systems [6, 26, 130, 131], whereas in Cu-poor, but Au-dominated, hydrothermal systems, Se commonly occurs within the lattice of auriferous zoned pyrite phases [132] where it is typically associated with Cu.

By contrast, Te has a spatial affinity for pyrite phases which Chouinard et al. attribute to its preferential incorporation into cubic crystal systems (Figure 9) [133]. However, Te can also occur in rare telluride phases such as altaite that may form micro-inclusions within pyrite phases (Figure 10) such as documented from the Birgilda porphyry Cu deposit in southern Urals, Russia [27].

7. Exploration of Porphyry Systems

Due to the lack of recycling of critical metals at industrial scale [134], mining of known mineral deposits and potential new discoveries through global mineral exploration represent their almost universal source, at least in 2026. As discussed above, there are increasingly severe restrictions on mineral exploration and the time from discovery to mining is normally of the order of about 20 years [135]. Despite this, it is appropriate to concisely discuss exploration for porphyry systems to round out this paper.

Porphyry systems are considered as tier-1 mineral deposits and very attractive exploration targets. They typically occur in natural clusters [21, 41, 48], and, hence, most mining companies prefer brownfield exploration programs targeting in the vicinity of their operating mines rather than investing into higher risk greenfield exploration projects even if the latter may be potentially more rewarding [11]. However, increasingly declining discovery rates in mature and well-established porphyry districts such as the central Andes and the Highlands of Papua New Guinea [136] now demand a higher investment into greenfield projects targeting new and less well-endowed exploration frontiers.

Greenfield target generation teams typically focus on continental-, post-collisional- and/or island arc settings [40, 58, 137]. Metallogenically fertile arc segments are selected based on the geochemical composition of their magmatic host intrusions [71, 74, 138] with special emphasis on the structural intersections between major arc-parallel structural corridors and deep-seated lineaments [41, 45, 46, 48]. More specifically, within curvilinear fertile arcs such as the Central Andes, individual clusters porphyry systems are commonly located near the intersections between arc-parallel crustal-scale faults and highly oblique transform or accommodation faults [41, 48]. Other world-class porphyry clusters are structurally controlled by: (1) deep-seated lineaments such as Oyu Tolgoi, Mongolia [53], or (2) pull-apart basins such as Peschanka, Siberia [139].

Typically, porphyry systems are defined by positive 'bullseye' magnetic signatures such as at Bajo de la Alumbrera, Argentina [140] or by 'doughnut'-shaped magnetic anomalies such as at Peschanka, Russia [139], as well as at Mt. Milligan, Canada [141].

Porphyry clusters typically include both economic porphyry Cu–Au deposits and weakly mineralized and uneconomic systems, all of which are genetically associated with similar intrusions derived from the same fractionating magma chamber [50, 53]. Even the most advanced geophysical methods are unable to distinguish between barren and productive porphyry systems as both are defined by very similar magnetic and IP (Induced Polarization) anomalies [122]. Hence, once a new porphyry cluster has been discovered during greenfield exploration, each system of this cluster must be evaluated individually by systematic drilling [37].

The major mining companies exploring for hydrothermal mineral systems increasingly use AI-supported tools for their target generation [142, 143]. The benefit of implementing machine learning tools in mineral exploration is to support geologists in the analysis and interpretation of large geochemical and geophysical data sets commonly referred to as 'Big Data' [142, 144]. For example, Diaz-Rodriguez et al use a spatio-temporal machine learning model to predict the emplacement of concealed porphyry systems [40]. Mineral prospectivity modeling is also developing into an important means for spatially mapping the potential distribution of minerals from the province- to district- and deposit-scales [143, 145].

During exploration, companies should take into account the potential value of critical trace elements and understand their deportment so that future development of porphyry-type mineral operations can optimise the metallurgical plant design to enable the extraction of all valuable trace elements such as Se, In, Te, and Re in addition to the main metals such as Cu, Au, and Mo.

8. Summary and Conclusions

Porphyry-type mineral systems, of either Cu–Au and Mo–Cu associations, comprise low-grade, but high-tonnage, deposits that represent the main global endowments of Cu and Mo. Porphyry Cu–Au systems are normally associated with calc-alkaline or alkaline intrusions with intermediate compositions that formed in continental- or island-arc settings such as in the South American Andes or Indonesia. In contrast, porphyry Mo±Re–Cu systems are preferentially hosted by highly evolved high-K calc-alkaline intrusive stocks derived in post-collisional-arc

settings such as in the Altaid/Transbaikal-Mongolian collage and North China Craton.

Porphyry systems are of economic interest not only for their Cu and Mo but also because they host significant contents of precious (Au, Ag) and trace critical metals (Se, In, Te, Re) which are of increasing economic interest due to their critical role in the green energy transition. From a critical trace element perspective, porphyry systems can be considered as large S and Fe, rather than Cu and Mo, anomalies in that pyrite typically represents the largest percentage of all sulfide phases, whereas chalcopyrite and bornite combined are only more abundant in the centres of gold-rich alkaline systems. As pyrite is normally the dominant sulfide on a whole-deposit scale and can have high critical trace element contents, it is generally the host to the greatest endowment of critical trace metals and understanding the deportment of these metals in pyrite is vital.

As the only source of these critical metals outside of recycling is from new mines developed on the basis of mineral exploration, which is becoming increasingly more difficult, extraction of the critical trace metals is important. Understanding of the deportment of these metals in pyrite is essential to the design of metallurgical processing plants in current and future porphyry mining projects so that treatment of large volumes of pyrite that hosts the majority of critical trace metals (e.g., Se, In, Te) can assist in meeting increasing demand if the green energy transition continues.

Author Contributions

D.M.: Conceptualization; Visualization; Data curation; Formal analysis; Writing—original draft. D.I.G.: Conceptualization; Visualization; Data curation, Validation; Writing—review and editing. M.S.: Data curation, Validation, Writing—review and editing. C.Y.: Data curation, Writing—review and editing. L.Z.: Data curation, Writing—review and editing. All authors have read and agreed to the published version of the manuscript.

Funding

This work did not receive any funding.

Institutional Review Board Statement

Not applicable.

Informed Consent Statement

Not applicable.

Data Availability Statement

All data generated or analyzed during this study are included in this published article.

Acknowledgements

We are indebted to Xing-Yun Chen of CUGB for her assistance in organizing and formatting the References in this paper. Many thanks are due to Franco Pirajno and three anonymous reviewers for their critical and very constructive suggestions.

Conflict of Interest

The authors declare no conflict of interest. Given their editorial roles, M. Santosh (Senior Consultant) and Chengxue Yang (Executive Editor) had no involvement in the peer review of this paper and had no access to information regarding its peer-review process. Full responsibility for the editorial process of this paper was delegated to another editor of the journal.

Use of AI and AI-assisted Technologies

No AI tools were utilized for this paper.

References

1. Kelley, K.D.; Huston, D.L.; Peter, J.M. Toward an effective global green economy: The critical minerals mapping initiative (CMMI). *SGA Newslett.* **2021**, *48*, 1–5.
2. European Commission. *Study on the Critical Raw Materials for the EU 2023*: *Final Report*; Publications Office of the European Union: Luxembourg, 2023.
3. Liu, Z.; Wang, S.; Liu, B.; et al. Advanced oxidation processes for sustainable critical metals extraction and recovery: Mechanisms, applications, and future perspectives. *J. Environ. Chem. Eng.* **2025**, *13*, 120193.
4. Pandey, R.; Krmíček, L.; Müller D.; et al. Alkaline rocks and their economic and geodynamic significance through geological time. In *Alkaline Rocks: Economic and Geodynamic Significance through Geological Time*; Geological Society of London: London, UK, 2025; Volume 551.
5. Groves, D.I.; Santosh, M.; Zhang, L. Net zero climate remediations and potential terminal depletion of global critical metal resources: A synoptic geological perspective. *Geosyst. Geoenviron.* **2023**, *2*, 100136.
6. Funari, V.; Gomes, H.I.; Coppola, D.; et al. Opportunities and threats of selenium supply from unconventional and low-grade ores: A critical review. *Resour. Conserv. Recycl.* **2021**, *170*, 105593.
7. Nassar, N.T.; Kim, H.; Frenzel, M.; et al. Global tellurium supply potential from electrolytic copper refining. *Resour. Conserv. Recycl.* **2022**, *184*, 106434.
8. Ahmad, N.I.; Kar, Y.B.; Doroody, C.; et al. A comprehensive review of flexible cadmium telluride solar cells with back surface field layer. *Heliyon* **2023**, *9*, e21622.
9. He, X.; You, Y.; Li, W.; et al. The enrichment mechanism of indium in Fe-enriched sphalerite from the Bainiuchang Zn-Sn polymetallic deposit, SW China. *Ore Geol. Rev.* **2024**, *167*, 105981.
10. Ivanov, V.V.; Yushko-Zakharova, O.E. Rhenium. In *Siderophile and Chalcophile Rare Metals Geological Directory*; Nedra: Moscow, Russia, 1989; pp. 425–459.
11. Müller, D.; Groves, D.I.; Santosh, M. *Metallic Mineral Resources: The Critical Components for a Sustainable Earth*; Elsevier: Amsterdam, The Netherlands, 2024; 474 p.

12. Sinclair, W.D. Porphyry deposits. In *Mineral Deposits of Canada: A Synthesis of Major Deposit Types, District Metallogeny, the Evolution of Geological Provinces, and Exploration Methods*; Goodfellow, W. D., Ed.; Special Publication No. 5; Geological Association of Canada, Mineral Deposits Division: St. John's, NL, Canada, 2007; pp. 223–243.
13. Sillitoe, R.H. Porphyry copper systems. *Econ. Geol.* **2010**, *105*, 3–41.
14. Sun, W.; Huang, R.; Li, H.; et al. Porphyry deposits and oxidized magmas. *Ore Geol. Rev.* **2015**, *65*, 97–131.
15. Zhang, Q.; Tang, J.; Li, F.; et al. Petrogenesis of the Tiegeshan diorite porphyry in the Duolong ore district, Tibet: Implications for porphyry mineralization. *Ore Geol. Rev.* **2026**, *191*, 107207.
16. Simon, A.C.; Ripley, E.M. The role of magmatic sulfur in the formation of ore deposits. *Rev. Mineral. Geochem.* **2011**, *73*, 513–578.
17. Richards, J.P.; Mumin, A.H. Magmatic-hydrothermal processes within an evolving Earth: Iron oxide-copper-gold and porphyry Cu±Mo±Au deposits. *Geology* **2013**, *41*, 767–770.
18. Blundy, J.; Mavrogenes, J.; Tattitch, B.; et al. Generation of porphyry copper deposits by gas–brine reaction in volcanic arcs. *Nat. Geosci.* **2015**, *8*, 235–240.
19. Rezeau, H.; Jagoutz, O. The importance of H_2O in arc magmas for the formation of porphyry Cu deposits. *Ore Geol. Rev.* **2020**, *126*, 103744.
20. Audetat, A.; Li, W. The genesis of Climax-type porphyry Mo deposits: Insights from fluid inclusions and melt inclusions. *Ore Geol. Rev.* **2017**, *88*, 436–460.
21. Heinrich, C.A. The chain of processes forming porphyry copper deposits. *Econ. Geol.* **2024**, *119*, 741–769.
22. Cioacă, M.E.; Munteanu, M.; Qi, L.; et al. Trace element concentrations in porphyry copper deposits from Metaliferi Mountains, Romania: A reconnaissance study. *Ore Geol. Rev.* **2014**, *63*, 22–39.
23. McFall, K.; Roberts, S.; Teagle, D.; et al. The origin and distribution of critical metals (Pd, Pt, Te and Se) within the Skouries Cu–Au porphyry deposit, Greece. *Trans. Inst. Min. Metall. Sect. B* **2016**, *125*, 100–101.
24. Rivas-Romero, C.; Reich, M.; Barra, F.; et al. The relation between trace element composition of Cu-(Fe) sulfides and hydrothermal alteration in a porphyry copper deposit: Insights from the Chuquicamata underground mine, Chile. *Minerals* **2021**, *11*, 671.
25. Steadman, J.; Large, R.; Olin, P.; et al. Pyrite trace element behavior in magmatic-hydrothermal environments: An LA-ICPMS imaging study. *Ore Geol. Rev.* **2021**, *128*, 103878.
26. Brodbeck, H.; McClenaghan, S.H.; Kamber, B.S.; et al. Metal(loid) deportment in sulfides from the high-grade core of the Bingham Canyon porphyry Cu-Mo-Au deposit, Utah. *Econ. Geol.* **2022**, *117*, 1521–1524.
27. Plotinskaya, O.Y.; Azovskova, O.B.; Belogub, E.V. Telluride mineralogy in ores of the Birgilda porphyry copper deposit (South Urals, Russia). *Geol. Ore Depos.* **2025**, *67*, 799–811.
28. Fathollahzadeh, H.; Mena, J.C.; Jowitt, S.M. Assessing the geochemical anomalies of bismuth, gallium, indium, and tellurium in the Río Blanco porphyry Cu-Mo deposit, central Chile; implications for the critical mineral and metal potential of porphyry copper systems. *Miner. Depos.*, **2026**, *61*, 775–782.
29. Jin, Y.; Xie, G.; Mao, J.; et al. The behavior of Se and Te during porphyry Cu-associated magmas evolution in the Middle-Lower Yangtze River metallogenic belt. *Lithos* **2026**, *523*, 108364.
30. Whitworth, A.J.; Vaughan, J.; Southam, G.; et al. Review on metal extraction technologies suitable for critical metal recovery from mining and processing wastes. *Miner. Eng.* **2022**, *182*, 107537.
31. Sun, Z.; Wu, J.; Cheng, H.; et al. Research progress on the extraction of strategic critical metals and the high value utilization of major element silicon from bulk mineral-metallurgical solid waste. *J. Environ. Chem. Eng.* **2025**, *13*, 118119.
32. Restivo, J.; Souza, J.P.S. Closed-loop mining waste management: Modification of clay byproducts for recovery of heavy metals from acid mine drainage. *Colloids Surf. A: Physicochem. Eng. Asp.* **2026**, *737*, 139736.
33. Viola, V.O.; Fernandes de Aquino, T.; Bonetti, B.; et al. Treatment of acid mine drainage (AMD) from the Santa Catarina Basin (Brazil) to retrieve rare earth. *J. Water Process Eng.* **2026**, *82*, 109549.
34. Zeng, L.; Deng, S.; Pan, Y.; et al. Sustainable preparation of battery-grade $FePO_4{\cdot}H_2O$ from acid mine drainage through a precipitation-purification pathway. *Resour. Conserv. Recycl.* **2026**, *225*, 108643.
35. Berzina, A.N.; Sotnikov, V.I.; Economou-Eliopoulos, M.; et al. Distribution of rhenium in molybdenite from porphyry Cu–Mo and Mo–Cu deposits of Russia (Siberia) and Mongolia. *Ore Geol. Rev.* **2005**, *26*, 91–113.
36. Lausberg, E.; Brugger, J.; Ram, R.; et al. Wasting the risk, or risking the waste? Understanding the trends of critical raw material loss into waste streams during copper and aluminium processing. *Resour. Conserv. Recycl.* **2026**, *228*, 108803.
37. Groves, D.I.; Santosh, M.; Müller, D.; et al. Mineral systems: Their advantages in terms of developing holistic genetic models and for target generation in global mineral exploration. *Geosyst. Geoenviron.* **2022**, *1*, 100001.
38. Zhang, L.; Groves, D.I.; Deng, J.; et al. Gold: From birth in neutron star collisions to human exploitation on Earth's crust. *Ore Geol. Rev.* **2025**, *187*, 106966.
39. Garwin, S.; Hall, R.; Watanabe, Y. Tectonic setting, geology, and gold and copper mineralization in Cenozoic magmatic arcs of southeast Asia and the west Pacific. *Econ. Geol.* **2005**, *100*, 891–930.
40. Diaz-Rodriguez, J.; Müller, R.D.; Chandra, R. Predicting the emplacement of cordilleran porphyry copper systems using a spatio-temporal machine learning model. *Ore Geol. Rev.* **2021**, *137*, 104300.
41. Rabbia, O. Metal endowment and fertility of Andean porphyry-copper belts. *Ore Geol. Rev.* **2026**, *190*, 107153.
42. Hedenquist, J.W.; Harris, M.; Camus, F. Geology and genesis of major copper deposits and districts of the world: A tribute to Richard H. Sillitoe. *Econ. Geol. Spec. Publ.* **2012**, *16*, 1–618.
43. Groves, D.I.; Santosh, M. *Mineral Systems, Earth Evolution, and Global Metallogeny*; Elsevier: Amsterdam, The Netherlands, 2023; 251 p.
44. Sillitoe, R.H.; Perello, J. Andean copper province: Tectonomagmatic settings, deposit types, metallogeny, exploration, and discovery. *Econ. Geol.* **2005**, *100*, 845–890.
45. Gow, P.A.; Walshe, J.L. The Role of preexisting geologic architecture in the formation of giant porphyry-related Cu±Au deposits: Examples from New Guinea and Chile. *Econ. Geol.* **2005**, *100*, 819–833.
46. Salfity, J.A. Lineamentos transversales al rumbo andino en el noroeste argentino. In *Actas del IV Congreso Geológico Chileno*; Asociación Geológica de Chile: Antofagasta, Chile, 1985; Volume 2, pp. 119–137.
47. Camus, F.; Castelli, J.C. *Historia exploracion y geologia de los yacimientos metaliferos de Chile 900–2020*; Origo Ediciones: Santiago, Chile, 2021; 1338 p.
48. Pena, M.; Palma, G.; Comte, D.; et al. Upper-crustal architecture and transpressional controls in the formation of the El Abra, Radomiro Tomic, and Chuquicamata porphyry copper systems, northern Chile. *Ore Geol. Rev.* **2025**, *187*, 106956.
49. Matteini, M.; Mazzuoli, R.; Omarini, R.; et al. The geochemical variations of the upper Cenozoic volcanism along the Calama–Olacapato–El Toro transversal fault system in the central Andes (24°S). *Tectonophysics* **2002**, *345*, 211–227.
50. Urzua, F. Geology, Geochronology and Structural Evolution of La Escondida Copper District, Northern Chile. Ph.D. Thesis, University

of Tasmania, Dynnyrne, TAS, Australia, 2009.

51. Pollard, P.J.; Taylor, R.G. Paragenesis of the Grasberg Cu-Au deposit, Irian Jaya, Indonesia: Results from logging Section 13. *Miner. Depos.* **2002**, *37*, 117–136.
52. Dwyer, R.; Forster, D.B.; Simpson, B.; et al. Relationships between high-K magmas and Cu–Au porphyry deposits in the Macquarie Arc, Australia. *Geol. Soc. Spec. Publ.* **2025**, *551*, 259–300.
53. Crane, D.; Kavalieris, I. Geologic overview of the Oyu Tolgoi porphyry Cu-Au-Mo deposits, Mongolia. *Econ. Geol. Spec. Publ.* **2012**, *16*, 187–213.
54. Olson, N.H.; Dilles, J.H.; Kent, A.J.; et al. Geochemistry of the Cretaceous Kaskanak batholith and genesis of the Pebble porphyry Cu-Au-Mo deposit, SW Alaska. *Am. Mineral.* **2017**, *102*, 1597–1621.
55. Deng, J.; Wang, Q.F., Gao, L.; et al. Differential crustal rotation and its control on giant ore clusters along the eastern margin of Tibet. *Geology* **2021**, *49*, 428–432.
56. Wang, R.; Zhu, D.C.; Wang, Q.; et al. Porphyry mineralization in the Tethyan orogen. *Sci. China Earth Sci.* **2020**, *62*, 2042–2067.
57. Hao, H.; Park, J.W.; Zheng, Y.C.; et al. Role of chalcophile element fertility in the formation of the eastern Tethyan post-collisional porphyry Cu deposits. *Miner. Depos.* **2024**, *59*, 1579–1594.
58. Müller, D.; Groves, D.I. *Potassic Igneous Rocks and Gold-Copper Mineralization*, 5th ed.; Springer: Cham, Switzerland, 2019; 398 p.
59. Chang, J.; Audetat, A.; Pettke, T. The gold content of felsic to mafic potassic magmas. *Nat. Commun.* **2024**, *15*, 6988.
60. Corbett, G.J.; Leach, T.M. *Southwest Pacific Rim Gold-Copper Systems: Structure, Alteration, and Mineralization*; Society of Economic Geologists: Littleton, CO, USA, 1998; Volume 6, 240 p.
61. Yang, Z.; Cao, K. Post-collisional porphyry Cu deposits in Tibet: An overview. *Earth Sci. Rev.* **2024**, *258*, 104954.
62. Chen, Y.J.; Zhang, C.; Wang, P.; et al. The Mo deposits of Northeast China: A powerful indicator of tectonic settings and associated evolutionary trends. *Ore Geol. Rev.* **2017**, *81*, 602–640.
63. Li, Z.Z.; Qin, K.Z.; Li, G.M.; et al. Formation of the giant Chalukou porphyry Mo deposit in northern great Xing'an range, NE China. *Lithos* **2014**, *203*, 138–156.
64. Ludington, S.; Plumlee, G.S. *Climax-Type Porphyry Molybdenum Deposits*; U.S. Geological Survey Open-File Report 2009–1215; U.S. Geological Survey: Reston, VA, USA, 2009; pp. 1–16.
65. Zhong, J.; Chen, Y.J.; Pirajno, F. Geology, geochemistry and tectonic settings of the molybdenum deposits in South China: A review. *Ore Geol. Rev.* **2017**, *81*, 829–855.
66. Zeng, Q.; Liu, J.; Qin, K.; et al. Types, characteristics, and time–space distribution of molybdenum deposits in China. *Int. Geol. Rev.* **2013**, *55*, 1311–1358.
67. Carten, R.B.; White, W.H.; Stein, H.J. High-grade granite-related molybdenum systems: Classification and origin. *Geol. Assoc. Canada, Spec. Pap.* **1993**, *40*, 521–554.
68. Klemm, L.M.; Pettke, T.; Heinrich, C.A. Fluid and source magma evolution of the Questa porphyry Mo deposit, New Mexico, USA. *Miner. Depos.* **2008**, *43*, 533–552.
69. Yang, Y.F.; Chen, Y.J.; Piranjo, F.; et al. Evolution of ore fluids in the Donggou giant porphyry Mo system, East Qinling, China. *Ore Geol. Rev.* **2015**, *65*, 148–164.
70. Soloviev, S.G. Late Paleozoic high-K magmatism and related metallogeny of the Tien Shan orogenic belt, Central Asia. *Geol. Soc. Spec. Publ.* **2025**, *551*, 231–258.
71. Loucks, R.R. Distinctive composition of copper-ore-forming magmas. *Aust. J. Earth Sci.* **2014**, *61*, 5–16.
72. Bekaert, D.V.; Turner, S.J.; Broadley, M.W.; et al. Subduction-driven volatile recycling: A global mass balance. *Ann. Rev. Earth Planet. Sci.* **2021**, *49*, 37–70.
73. Waters, L.E.; Cottrell, E.; Coombs, M.L.; et al. Generation of calc-alkaline magmas during crystallization at high oxygen fugacity. *J. Petrol.* **2021**, *62*, egaa104.
74. Mafra, C.; Loucks, R.; Fiorentini, M. Distinctive source and hydration state of gold-ore-forming arc magmas. *Geology* **2024**, *53*, 195–200.
75. Bao, X.S.; Yang, L.Q., He, W.Y.; et al. Importance of magmatic water content and oxidation state for porphyry-style Au mineralization: An example from the giant Beiya Au deposit, SW China. *Minerals* **2018**, *8*, 441.
76. Richards, J.P. Porphyry copper deposit formation in arcs: What are the odds? *Geosphere* **2022**, *18*, 130–155.
77. Lamont, T.N.; Loader, M.A.; Roberts, N.M.; et al. Porphyry copper formation driven by water-fluxed crustal melting during flat-slab subduction. *Nat. Geosci.* **2024**, *17*, 1306–1315.
78. Lee, C.T.; Leeman, W.P.; Canil, D.; et al. Similar V/Sc systematic in MORB and arc basalts: Implications for the oxygen fugacities of their mantle source regions. *J. Petrol.* **2005**, *46*, 2313–2336.
79. Halter, W.E.; Pettke, T.; Heinrich, C.A. The origin of Cu/Au ratios in porphyry type ore deposits. *Science* **2002**, *296*, 1844–1846.
80. Audetat, A.; Chang, J.; Gaynor, S.P. Depth of magma crystallization and fluid exsolution beneath the porphyry-skarn Cu deposits at Santa Rita and Hanover-Fierro, New Mexico, USA. *Econ. Geol.* **2025**, *120*, 1679–1699.
81. Murakami, H.; Seo, J.K.; Heinrich, C.A. The relation between Cu/Au ratio and formation depth of porphyry-style Cu-Au±Mo deposits. *Miner. Depos.* **2009**, *45*, 11–21.
82. Weis, P.; Driesner, T.; Heinrich, C.A. Porphyry-copper ore shells form at stable pressure-temperature fronts within dynamic fluid plumes. *Science* **2012**, *338*, 1613–1616.
83. Cao, M.J.; Qin, K.Z.; Li, G.M.; et al. Oxidation state inherited from the magma source and implications for mineralization: Late-Jurassic to Early-Cretaceous granitoids, central Lhasa subterrane, Tibet. *Miner. Depos.* **2018**, *53*, 299–309.
84. Lee, R.G.; Dilles, J.H.; Tosdal, R.M.; et al. Magmatic evolution of granodiorite intrusions at the El Salvador porphyry copper deposit, Chile. *Econ. Geol.* **2017**, *112*, 245–273.
85. Richards, J.P. Post-subduction porphyry Cu-Au and epithermal Au deposits: Products of remelting of subduction-modified lithosphere. *Geology* **2009**, *37*, 247–250.
86. Zhong, S.; Feng, C., Seltmann, R.; et al. Geochemical contrasts between late Triassic ore-bearing and barren intrusions in the Weibao Cu-Pb-Zn deposit, east Kunlun Mountains, NW China. *Miner. Depos.* **2018**, *53*, 855–870.
87. Richards, J.P. Alkalic-type epithermal gold deposits: A review. In *Magmas, Fluids, and Ore Deposits*; Thompson, J.F.H., Ed.; Mineralogical Association of Canada Short Course Series; Mineralogical Association of Canada: Toronto, ON, Canada, 1995; Volume 23, pp. 367–400.
88. Williams, H.M.; Prytulak, J.; Woodhead, J.D.; et al. Interplay of crystal fractionation, sulfide saturation and oxygen fugacity on the iron isotope composition of arc lavas: An example from the Marianas. *Geochim. Cosmochim. Acta* **2018**, *226*, 224–243.
89. Halley, S. Mapping magmatic and hydrothermal processes from routine exploration geochemical analyses. *Econ. Geol.* **2020**, *115*, 489–503.
90. Voudoulis, P.; Mavroganatos, C.; Spry, P.; et al. Porphyry and epithermal deposits in Greece: An overview, new discoveries, and mineralogical constraints on their genesis. *Ore Geol. Rev.* **2019**, *107*, 654-691.
91. Portela, B.; Sepp, M.D.; van Ruitenbeek, F.J.A.; et al. Using hyperspectral imagery for identification of sillitoeboucherpyrophyllite-muscovite intergrowths and alunite in the shallow epithermal environment of the Yerington porphyry copper district. *Ore Geol. Rev.* **2021**, *131*, 104012.

92. Heinrich, C.A. The physical and chemical evolution of low-salinity magmatic fluids at the porphyry to epithermal transition: A thermodynamic study. *Miner. Depos.* **2005**, *39*, 864–889.
93. Saber, E.S.; El-Wahed, M.A.; El-Sheikh, A.; et al. Fertile high-K magmatism and hydrothermal alteration zone associated with porphyry copper mineralization in the Samra area, SE Sinai, Egypt. *Sci. Rep.* **2025**, *15*, 44223.
94. Mpodozis, C.; Cornejo, P. Cenozoic tectonics and porphyry copper systems of the Chilean Andes. *Econ. Geol. Spec. Publ.* **2012**, *16*, 329–360.
95. McInnes, B.I.; Evans, N.J.; Fu, F.Q.; et al. Application of thermochronology to hydrothermal ore deposits. *Rev. Mineral. Geochem.* **2005**, *58*, 467–498.
96. Barley, M.E. Porphyry-style mineralization associated with early Archean calc-alkaline igneous activity, eastern Pilbara, Western Australia. *Econ. Geol.* **1982**, *77*, 1230–1236.
97. Turner, S.J.; Reynolds, J.; Hagemann, S.G. Boddington: An enigmatic giant Archean gold-copper (molybdenum-silver) deposit in the southwest Yilgarn Craton, Western Australia. *Econ. Geol. Spec. Publ.* **2020**, *23*, 275–288.
98. Outteridge, T.; Kinsman, N.; Ronchi, G.; et al. Industrial relevance of molybdenum in China. *Adv. Manuf.* **2020**, *8*, 35–39.
99. Liu, L.; Zhang, L.; Jiang, S.; et al. Global copper cycles in the anthroposphere since the 1960s. *Resour. Conserv. Recycl.* **2023**, *199*, 107294.
100. Youngman, T.H.; Nielsen, R.; Crovetto, A.; et al. Semitransparent selenium solar cells as a top cell for tandem photovoltaics. *Sol. RRL* **2021**, *5*, 2100111.
101. Liu, F.W.; Cheng, T.M.; Chen, Y.J.; et al. High-yield recycling and recovery of copper, indium, and gallium from waste copper indium gallium selenide thin-film solar panels. *Sol. Energy Mater. Sol. Cells* **2022**, *241*, 111691.
102. Cerchiaro Sanchez, I. Critical Minerals in Copper and Molybdenum-Tungsten Deposits Associated with Laramide-age Intrusions of the Hillsboro and Eureka Districts, and Paleogene-age Victorio and Tres Hermanas Districts, New Mexico. Master's Thesis, New Mexico Institute of Mining and Technology, Socorro, NM, USA, 2025.
103. Chivers, T.; Laitinen, R.S. Tellurium: A maverick among the chalcogens. *Chem. Soc. Rev.* **2015**, *44*, 1725–1739.
104. Albarede, F. *Geochemistry*; Cambridge University Press: Cambridge, UK, 2013; 342 p.
105. Rumble, J. R., Ed. *CRC Handbook of Chemistry and Physics*, 102nd ed.; CRC Press: Boca Raton, FL, USA, 2021; 1550 p.
106. Wu, X.; Xie, G.; Xu, J.; et al. Distribution of Co, Te, Se in porphyry copper systems: A case study of the Tonglvshan deposit, Eastern China. *Ore Geol. Rev.* **2024**, *174*, 106304.
107. Graham, A.C.; Orovan, E.A.; Wall, C.; et al. *Data Release from Critical Mineral Studies of the Kitsault, Huckleberry, and Berg Porphyry Deposits*; British Columbia Geological Survey GeoFile, GeoFile 2025–23; British Columbia Ministry of Mining and Critical Minerals, British Columbia Geological Survey: Victoria, BC, Canada, 2025; pp. 1–11.
108. Singer, D.A.; Berger, V.I.; Moring, B.C. *Porphyry Copper Deposits of the World: Database and Grade and Tonnage Models*; U.S. Geological Survey Open-File Report 2008-1155; U.S. Geological Survey (USGS): Reston, VA, USA, 2008.
109. Rubin, J.N.; Kyle, J.R. Precious metal mineralogy in porphyry-, skarn-, and replacement-type ore deposits of the Ertsberg (Gunung Bijih) District, Irian Jaya, Indonesia. *Econ. Geol.* **1997**, *92*, 535–550.
110. George, L.L.; Cook, N.J.; Crowe, B.B.; et al. Trace elements in hydrothermal chalcopyrite. *Mineral. Mag.* **2018**, *82*, 59–88.
111. Seedorff, E.; Dilles, J.H.; Profett, J.M.; et al. Porphyry deposits: Characteristics and origin of hypogene features. *Econ. Geol.* **2005**, *100*, 251–298.
112. Vigneresse, J.L.; Poddar, A.; Chattaraj, P.K. Felsic trans-porphyry deposits and associated ore (Sn, Ta, Nb, pegmatites) viewed from physics, chemistry (cDFT) and geologic contexts. *Lithos* **2025**, *515*, 108200.
113. Landtwing, M., Pettke, T., Halter, W.E.; et al. Copper deposition during quartz dissolution by cooling magmatic–hydrothermal fluids: The Bingham porphyry. *Earth Planet. Sci. Lett.* **2005**, *235*, 229–243.
114. Sinclair, W.D.; Jonasson, I.R.; Kirkham, R.V.; et al. Rhenium in Canadian mineral deposits. In *Proceedings of the 24th International Applied Geochemistry Symposium*; International Association of Applied Geochemistry: Fredericton, NB, Canada, 2009; pp. 225–228.
115. Dai, J.Z.; Mao, J.W.; Yang, F.Q.; et al. Geological characteristics and geodynamic background of molybdenum (copper) deposits along Yanshan–Liaoning metallogenic belt at the northern margin of North China block. *Miner. Depos.* **2006**, *25*, 598–615.
116. Voudouris, P.; Melfos, V.; Spry, P.G.; et al. Extremely Re-rich molybdenite from porphyry Cu-Mo-Au prospects in northeastern Greece: Mode of occurrence, causes of enrichment, and implications for gold exploration. *Minerals* **2013**, *3*, 165–191.
117. Ma, W.; Wen, H.; Zhou, Z.; et al. Vapor phase facilitated rhenium enrichment in porphyry Mo deposit: Insights from thermodynamic simulations and molybdenum isotopes at Jinduicheng deposit, central China. *J. Geochem. Explor.* **2026**, *286*, 108057.
118. Xiong, X.; Zhu, L., Yang, P.; et al. Texture, geochemistry and U–Pb geochronology of monazite of different origins: Implications for the magmatic–hydrothermal evolution of the Guilingou porphyry Mo-W deposit, South Qinling Orogen, central China. *Ore Geol. Rev.* **2025**, *182*, 106648.
119. Nie, X.T.; Sun, J.G., Sun, F.Y.; et al. Zircon U–Pb and molybdenite Re–Os dating and geological implications of the Shimadong porphyry molybdenum deposit in eastern Yanbian, northeastern China. *Can. J. Earth Sci.* **2020**, *57*, 630–646.
120. Liu, H.; Wang, J.; Chen, Q.; et al. Magmatic evolution and Nb-Ta enrichment of Early Jurassic granitic porphyry from the Shangxiahu Nb-Ta deposit of the Nanling Range, China. *Minerals* **2024**, *14*, 1005.
121. Qi, J.; Chi, G.; Tang, J.; et al. In-situ trace element and sulfur isotope analyses of sulfides as indicators of ore-forming fluid evolution in the Lakang'e porphyry Mo-Cu deposit, Tibet, China. *Ore Geol. Rev.* **2025**, *183*, 106690.
122. Berger, B.R.; Ayuso, R.A.; Wynn, J.C.; et al. *Preliminary Model of Porphyry Copper Deposits*; U.S. Geological Survey Open-File Report 2008-1321; U.S. Geological Survey: Reston, VA, USA, 2008; pp. 1–62.
123. Nielsen, R.L. Hypogene texture and mineral zoning in a copper-bearing granodiorite stock, Santa Rita, New Mexico. *Econ. Geol.* **1968**, *63*, 37–50.
124. Gustafson, L.B.; Hunt, J.P. The porphyry Cu deposit at El Salvador, Chile. *Econ. Geol.* **1976**, *70*, 857–912.
125. John, E.C. Mineral zones in the Utah Copper orebody. *Econ. Geol.* **1978**, *73*, 1250–1259.
126. Bogdanov, K. Pyrite and chalcopyrite as minerals-vectors toward porphyry-epithermal systems. In *Abstracts of the National Conference "GEOSCIENCES 2015"*; Bulgarian Geological Society: Sofia, Bulgaria, 2015; pp. 13–14.
127. Boucher, B.M.; Robb, S.J.; Hanley, J.J.; et al. Platinum-group elements (PGE) in the New Afton alkalic Cu-Au porphyry deposit, Canadian Cordillera, I: Relationships between PGE, accessory metals and sulfur isotopes in pyrite. *Front. Earth Sci.* **2023**, *11*, 819129.
128. Keith, M.; Smith, D.J.; Jenkin, G.R.; et al. A review of Te and Se systematics in hydrothermal pyrite from precious metal deposits: Insights into ore-forming processes. *Ore Geol. Rev.* **2018**, *96*, 269–282.

129. Xiao, X.; Zhou, T.; Hollings, P.; et al. Pyrite geochemistry in a porphyry-skarn Cu (Au) system and implications for ore formation and prospecting: Perspective from the Xinqiao deposit, Eastern China. *Am. Mineral.* **2023**, *108*, 1132–1148.
130. Wang, C.; Li, S.; Wang, H.; et al. Selenium minerals and the recovery of selenium from copper refinery anode slimes. *J. South. Afr. Inst. Min. Metall.* **2016**, *116*, 593–600.
131. Martin, A.J.; McDonald, I.; MacLeod, C.J.; et al. Extreme enrichment of selenium in the Apliki Cyprus-type VMS deposit, Troodos, Cyprus. *Mineral. Mag.* **2018**, *82*, 697–724.
132. Chen, J.; Huang, Z.L., Yang, R.D.; et al. Gold and antimony metallogenic relations and ore-forming process of Qinglong Sb-(Au) deposit in Youjiang basin, SW China: Sulfide trace elements and sulfur isotopes. *Geosci. Front.* **2021**, *12*, 605–623.
133. Chouinard, A.; Paquette, J.; William-Jones, A.E. Crystallographic controls on trace-element incorporation in auriferous pyrite from the Pascua epithermal high-sulfidation deposit: Chile-Argentina. *Can. Mineral.* **2005**, *43*, 951–963.
134. Müller, D.; Groves, D.I.; Zhang, L. Towards a circular economy: Modern recycling technologies for critical metals. *Gondwana Res.* **2026**, *152*, 80–91.
135. Schodde, R. Time delay between discovery and development—Is it becoming more difficult? Presented at the China Mining 2017 Conference, Tianjin, China, 23 September 2017.
136. Guj, P.; Schodde, R. Will future copper resources and supply be adequate to meet the net zero emission goal? *Geosyst. Geoenviron.* **2025**, *4*, 100320.
137. Wu, C.; Chen, H.; Chiaradia, M.; et al. Linking Pacific Plate formation and Early Cretaceous metallogenic response on the circum-Pacific continental margins. *GSA Bull.* **2023**, *136*, 171–183.
138. Cocker, H.A.; Valente, D.L.; Park, J.W.; et al. Using platinum group elements to identify sulfide saturation in a porphyry Cu system: The El Abra porphyry Cu deposit, northern Chile. *J. Petrol.* **2016**, *56*, 2491–2514.
139. Chitalin, A.F.; Baksheev, I.A.; Nikolaev, Y.N.; et al. *Porphyry Cu–Au±Mo Mineralization Hosted by Potassic Igneous Rocks: Implications from the Giant Peschanka Porphyry Deposit, Baimka Trend (North East Siberia, Russia)*; Geological Society of London: London, UK, 2022; Volume 513, pp. 323–349.
140. Clark, D.A. Magnetic effects of hydrothermal alteration in porphyry copper and iron-oxide copper–gold systems: A review. *Tectonophysics* **2014**, *625*, 46–65.
141. Kwan, K.; Müller, D. Mount Milligan alkalic porphyry Au-Cu deposit, British Columbia, Canada, and its AEM and AIP signatures: Implications for mineral exploration in covered terrains. *J. Appl. Geophys.* **2020**, *180*, 104131.
142. Yang, F.; Zuo, R.; Kreuzer, O. Artificial intelligence for mineral exploration: A review and perspectives on future directions from data science. *Earth-Sci. Rev.* **2024**, *258*, 104941.
143. Davies, R.S.; Trott, M.; Georgi, J.; et al. Artificial intelligence and machine learning to enhance critical mineral deposit discovery. *Geosyst. Geoenviron.* **2025**, *4*, 100361.
144. Ning, Y.; Wang, Y., Lu, J.; et al. Mineral prospectivity mapping for multi-source geoscience data: A novel unsupervised deep learning method. *Ore Geol. Rev.* **2025**, *186*, 106866.
145. Mitra, S.; Mallick, S.; Biswas, S.; et al. Advanced machine learning based gold prospectivity mapping in the Dharwar Craton, India: A hybrid knowledge-data driven paradigm integrating ensemble and deep learning. *Geosyst. Geoenviron.* **2026**, *5*, 100473.